Characterization of aerosolized particles in effluents from carbon fibre composites incorporating nanomaterials during simultaneous fire and impact

Robert Chapple, C. Chivas-Joly, Jean Claude Roux, Loïc Dumazert, Laurent Ferry, J. Lopez-Cuesta, E.L. Erskine, B.K. Kandola

NanoImpact 29 (2023) 100446

Contents lists available at ScienceDirect

NanoImpact

journal homepage: www.elsevier.com/locate/nanoimpact

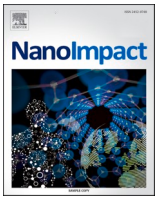

Characterization of aerosolized particles in effluents from carbon fibre composites incorporating nanomaterials during simultaneous fire and impact

R. Chapple [a], C. Chivas-Joly [b], J.-C. Roux [c], L. Dumazert [c], L. Ferry [c], J.-M. Lopez-Cuesta [c], E.L. Erskine [d], B.K. Kandola [a,*]

[a] IMRI, University of Bolton, Deane Road, Bolton BL3 5AB, UK
[b] LNE, CARMEN Platform, DMSI, 29 Avenue Roger Hennequin, 78197 Trappes, France
[c] PCH, IMT Mines Ales, 6 Avenue de Clavières 30319 Alès Cedex, France
[d] Dstl, Porton Down, Salisbury SP4 0JQ, UK

ARTICLE INFO

Editor: Bernd Nowack

Keywords:
Carbon fibre composites
Nanomaterials
Impact and fire
Aerosol
Soot

ABSTRACT

This work investigates the aerosols emitted from carbon fibre-reinforced epoxy composites (CFC) incorporating nanomaterials (nanoclays and nanotubes), subjected to simultaneous fire and impact, representing an aeroplane or automotive crash. Simultaneous fire and impact tests were performed using a previously described bespoke testing methodology with the capability to collect particles released from the front/back faces of the impacted composites plus the effluents. In this work the methodology has been further developed by connecting the Dekati Low Pressure Impactor (DLPI) and Mini Particle Sampler (MPS) sampling system in the extraction chimney. The aerosols emitted have been characterized using various devices devoted to the analysis of aerosols. The influence of the nanoadditives in the matrix on the number concentration and the size distribution of airborne particles produced, was studied with a cascade impactor in the 5 nm–10 μm range. The morphology of the separated soot fractions was examined by SEM. The measurement of aerodynamic size of particles that can deposit in human respiratory tract indicate that 75% of the soot and particles released from CFC could deposit in the lungs reaching the bronchi region at a minimum. There was however, a minimal difference between the number particle concentrations or particle-size mass distribution of particles from CFC and CFC containing nanoadditives. Moreover, no fibres were found in the effluents.

1. Introduction

Carbon fibre - reinforced epoxy composites (CFC) are important structural materials for aerospace, transportation, sporting equipment and other industrial applications because of their excellent mechanical properties in tensile and flexural modes (Zhang et al., 2016; Holmes, 2014; Souto et al., 2018). However, their poor fracture toughness has always been a major issue (Li et al., 2020; Ning et al., 2022), mainly due to brittle nature of the epoxy matrix. Hence matrix toughening is the most commonly employed method to improve fracture toughness of the composite (Shrivastava and Singh, 2020). Typically nanomaterials (International Organization for Standardization, ISO/TS 27,687:2008, 2008) such as nanoclays, nanotubes and graphene are used to reinforce the polymeric matrix (Zabihi et al., 2018; Shettar et al., 2020; Bai, 2003; Liu et al., 2012), which improve the matrix dominant properties of the composite, including fracture toughness (Zabihi et al., 2018). Owing to their low densities and large specific surface areas, these nanomaterials are effective at low concentrations (< 5 wt%). Another major concern for CFCs is the intrinsic flammability of the organic polymeric matrix. The epoxy resin on exposure to heat, undergoes decomposition at temperatures >300 °C prior to combustion (Kandola and Kandare, 2008; Mouritz and Gibson, 2006), resulting in loss of structural integrity and mechanical failure. These nanomaterials also are known to improve the thermal stability of the resin and impart fire retardancy to a certain extent (Martins et al., 2016; Kalali et al., 2016; Kandola and Deli, 2014).

In a fire event, particularly in post-fire crash scenarios, there are also health risks as when the organic matrix of the composite decomposes, gaseous species and aerosols containing nanomaterials and nano/micro

* Corresponding author.
E-mail address: B.Kandola@bolton.ac.uk (B.K. Kandola).

https://doi.org/10.1016/j.impact.2022.100446
Received 20 September 2022; Received in revised form 30 November 2022; Accepted 6 December 2022
Available online 9 December 2022

sized carbon fibres are released into surrounding area and remain airborne (Morrey, 2001). There are many reports of aeroplane crashes where rescue team working on the site suffered with serious 'needle-stick' injuries, respiratory problems, eye and skin irritation, headaches and nausea (La Delfa et al., 2009; Costantino et al., 2015). Even after several days of the crash, members of the recovery team experienced discomfort including sore eyes, throat and chests and skin irritation (Mouritz and Gibson, 2006; Morrey, 2001; La Delfa et al., 2009). Most of these problems have been linked to small carbon fibre pieces, released from the main body of the composite, which in fire and air, get oxidised, getting to nano-sized and sharp enough to puncture human skin, and small enough to be inhaled and carried down the trachea into the lungs (Mouritz and Gibson, 2006; Morrey, 2001; La Delfa et al., 2009; Costantino et al., 2015; Hertzberg, 2005; Gandhi et al., 1999). Most of the toxicological studies for carbon fibres have been performed on virgin carbon fibres, showing no adverse health effects (Owen et al., 1986; Thomson et al., 1990) or causing temporary lung inflammation that is reversible after 10–30 days (Waritz et al., 1990; Warheit et al., 1994; Zhang et al., 2006). However, during burning of a composite, the fibres released may be substantially different considering their potential contamination with various chemicals and combustion products from the polymer matrix. These absorbed chemicals may increase fibre retention or macrophage activity and inhibit the phagocytizing of the fibres (Gandhi, 1999). Although the focus of these concerns has previously been related to military applications, the increased use of CFCs in the commercial transportation sector, causes greater concern for the general public currently and in the future.

There is strong probability that the biological activity of released particulates especially those defined as nanomaterials is dependent on physicochemical parameters: size, distribution, aggregation/agglomeration state, shape, crystal structure, chemical composition, surface area, surface chemistry, surface charge, and solubility/dispersibility (Oberdörster et al., 2005). Particles with an aerodynamic diameter <10 μm can be inhaled directly through the respiratory tract and into the lung by humans (Winter-Sorkina and Cassee, 2002), the deposition of particles in human respiratory tract, however depends on sedimentation and Brownian motion of the particles. Thus, CFCs containing nanomaterials could present a greater health risk when released as they may reach the deepest regions of the lung. To understand the distribution and toxicity of soot and particles once inside the respiratory tract, it is first important to understand their morphology by taking representative samples from effluent in controlled laboratory conditions.

Previously a few studies have been performed to characterise aerosols for nanosized materials and gaseous products released from burning composites (Nyden et al., 2009; Motzkus et al., 2010; Chivas-Joly et al., 2013; Fleury et al., 2011; Chivas-Joly et al., 2019; Sotiriou et al., 2015; Singh et al., 2016; Schlagenhauf et al., 2015), none of these though involved impact scenario. In that context we recently developed a methodology where CFCs can be exposed to simultaneous radiant heat/fire and impact, and all the released particles from the back and front surfaces of the impacted composite and from the effluents can be collected (Chapple et al., 2021). The morphological characterization of the particles captured from the front and back faces of the CFC without/with nanomaterials, subjected to 50 and 75 kW/m^2 heat fluxes (using a cone calorimetric heater, ISO 5660) and 19 J impact was used to predict their potential deposition in lungs and any subsequent physiological harm that may be caused during human exposure and especially after the exposure (Chapple et al., 2022). These experimental parameters were established during research and development of the bespoke equipment following guidance from standard cone calorimetry (ISO 5660) and low velocity drop-weight impact testing. These heat flux and impact energy combination provide sufficient heating/consistent ignition of sample and impact damage of a degree that releases a substantial amount of particulates (Chapple et al., 2021), In this work the methodology has been further developed to identify and characterise aerosols by attaching a cascade impactor and a particle sampler system in the chimney of the bespoke equipment. Cascade impactors are a methodology that collect particles in different size fractions according to their inertial properties in a moving air stream. The deposition of particles is based on the particle's aerodynamic diameter and inertia, which are relevant parameters for predicting particle transport and deposition within the respiratory tract (Majoral et al., 2006).

2. Experimental

2.1. Composite materials

Materials: A low-viscosity and room-temperature curing epoxy resin containing diglycidyl ether of bisphenol A/F resin (Epilok 60–822 resin, Bitrez Ltd., UK.) and an amine-based hardener (Curamine 32–790 NT, Bitrez Ltd., UK). Nanomaterials included a nanoclay (NC), octadecyl ammonium ion-modified montmorillonite clay (Nanomer I.30E, Nanocor Inc., China); layered double hydroxides (LDH), unmodified synthetic hydrotalcite (magnesium aluminium hydroxycarbonate (Sigma Aldrich); carbon nanotubes (NT), single wall carbon nanotubes (Tuball 301, OCSiAL Luxembourg). Reinforcement included woven carbon fabrics (Mitsubishi TR30S, 3 K, 0/90° 2 × 2 twill weave, 200 Tex, ρ = 1.79 g/cm^3, filament diameter 7 μm, sourced from East Coast Fiberglass, UK).

CFCs were prepared by mixing the epoxy resin and curing agent in 100:38 wt% ratio and mechanically-stirring for about 5 min. Air bubbles were removed by degassing in a vacuum chamber. Resin was infused into 10 plies of 300 mm × 300 mm sized carbon fibres by resin infusion, cured at room temperature for 24 h, followed by post curing in oven at 80 °C for 8 h. To fabricate composites with nanomaterials, resins with pre-dispersed nanomaterials at required concentrations (see Table 1) by high shear mixing method (turbo-mixer) at Bitrez Ltd., were used, following the methodology as for CFC. Sample details are given in Table 1. The composite laminates were cut into samples of sizes 100 mm × 100 mm by band saw for testing.

2.2. Experimental setup

The design and operational details of the bespoke testing equipment for simultaneous impact and fire testing through a pendulum impactor coupled with a radiant heat source (cone heater), and capturing of released particle at the front and back faces, have been described in details in our previous publication (Chapple et al., 2021), the schematic of the equipment is shown in Fig. 1 (coloured grey). A Dekati Low Pressure Impactor (DLPI) and an Ecomesure Mini Particle Sampler (MPS) were attached to the chimney of the cone heater to capture submicron sized particles as shown in Fig. 1 (coloured green).

The DLPI is a 13-stage cascade low pressure impactor used to determine particle-size mass distribution (Fig. S1(a)). The multi-stage aerosol-sampling device separates particles by size, according to their inertial properties in a moving air stream. The inertia of a particle is function of its diameter, shape, density and velocity. The most common

Table 1
Composite sample composition.

Sample	Nanomaterial Type	Nanomaterial conc. in resin wt %	Fibre weight fraction (FWF) wt%	Thickness (mm)
CFC	–	–	63.6	2.36 ± 0.04
CFC_NC	Nanoclay (Nanomer I.30E)	5.0	65.2	2.30 ± 0.04
CFC_LDH	Layered double hydroxide	5.0	63.6	2.43 ± 0.02
CFC_NT	Single wall carbon nanotubes	0.3	63.7	2.45 ± 0.01

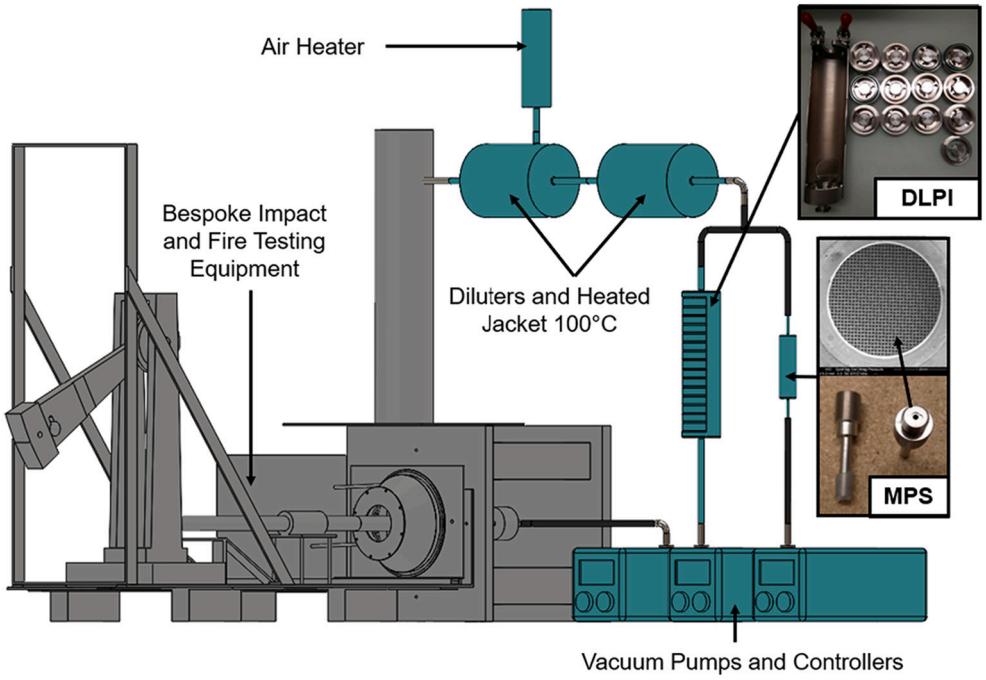

Fig. 1. (a) Detailed CAD schematic and images of the complete DLPI/MPS set-up (green coloured) combined with the bespoke impact and fire equipment (grey coloured), (b) image of the MPS TEM grid. (For interpretation of the references to colour in this figure legend, the reader is referred to the web version of this article.)

equivalent particle size is the aerodynamic particle diameter, defined as the diameter of a spherical unit-density particle (=1000 kg.m^{-3}) with the same gravitational settling velocity as the particle under consideration (Kulkarni et al., 1993; International Organization for Standardization, ISO 29904, 2013). The aerosol flow system transports the particles and collects the particles on a surface (e.g. a filter). The aerosol enters through succeeding orifice stages with higher orifice velocity than the last stage. The deposition of the particles or impacting particles on each stage are collected on a filter surface (Fig. S1(b)). Each stage of the impactor is characterized by the cut-off diameter size and noted $D_{50\%}$ corresponding to the aerodynamic diameter of particles trapped with and efficiency of 50%. This process separates the particles into size ranges as a function of their mass (Fig. S1(c)) (Rhodes et al., 2011). The size classification range of the DLPI is from 30 nm to 10 μm, the collection plate within each impact stage requires an impaction substrate (Dekati, 2022).

CFC samples without/with nanomaterials were subjected to (i) 75 kW/m^2 heat exposure only and (ii) 75 kW/m^2 heat exposure and 16 J impact 10 s after time-to-ignition (TTI + 10 s). 75 kW/m^2 heat flux was chosen to ensure that the sample auto-ignites, replicating a fire situation. Sampling of effluents with the DLPI was initiated as the cone heater was located in place to expose the sample to radiant heat. The sampling was continued throughout the experiment until 120 s after flame out (FO) in which effluents were no longer visibly released. The cone heater was removed 60 s after FO. In parallel, the MPS was used to sample a small concentration of soot and particles in the size range of 1 nm to 1 μm. The MPS required a 3 mm circular Copper Quantifoil 400 mesh/1.2 μm grid for this sampling. A new grid was fitted to the MPS after each sampling. To determine when to take MPS samples, the smoke production rate (SPR) measurements as a function of time (Fig. 2) were recorded for the control CFC sample by the bespoke impact and fire equipment using the smoke obscuration measuring system of a standard cone calorimeter using the attenuation of the laser beam. As can be seen from Fig. 2 there was a first peak of effluent evolution at ignition, based on which the first MPS sampling was initiated at ignition. In the SPR vs time curve, a second peak was identified at approximately 250 s and a second MPS sample was taken to compare against the sample at ignition.

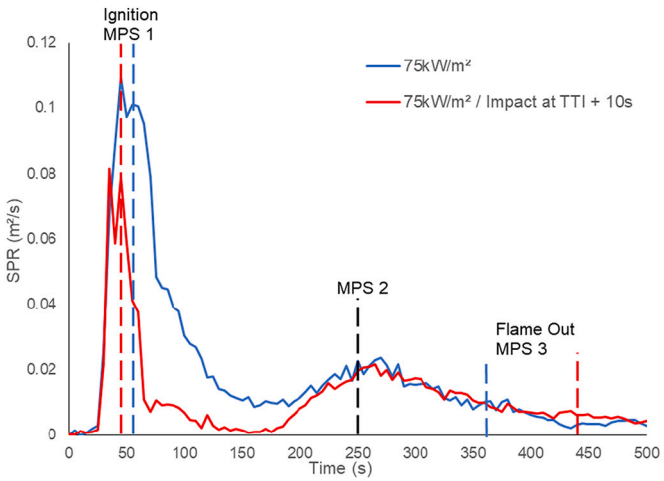

Fig. 2. Smoke production rate (SPR) versus time curves for CFC sample during 75 kW/m^2 heat exposure and impact at TTI + 10 s during 75 kW/m^2 heat exposure recorded by the smoke obscuration measuring system of a standard cone calorimeter.

A third sample was taking at FO for a final comparison to check. If the duration of time sampling with the MPS was too high, it would result in a high concentration of soot on the Quantifoil grid, making it difficult to characterise any particulates on them. For this reason, the sampling duration was 20 s from ignition, during 75 kW/m^2 heat exposure, and impact at TTI + 10 s during 75 kW/m^2 heat exposure. This was to allow the impact event to occur at the mid-point of the MPS sampling. The importance of sampling at impact was to investigate if other particle types, for example resin particles, fibres and particularly nanomaterial additives, could be captured within the effluents. The second MPS sample at 250 s and the third at FO were also performed for 20 s for consistency. The debris and particles released from the front and back faces were also captured in respective chambers as detailed elsewhere (Chapple et al., 2021; Chapple et al., 2022).

For accurate gravimetric analysis, Millipore 0.2 μm, 25 mm diameter polycarbonate filter substrates fitted in each DLPI impaction stages and in the back face chamber (details in ref. (Chapple et al., 2021; Chapple, 2021)), were weighed thrice to determine a precise average, using the Sartorius Quintix 65-1S analytical balance with a readability and reproducibility of 0.01 mg and ± 0.02 mg, respectively. For each test, before fitting the filters and assembling the impaction stages, the DLPI required cleaning with ethanol to reduce the possibility of contamination between tests. Post-test the DLPI was removed and dismantled carefully. Each filter was organised in specified petri dishes to transfer them for post-test gravimetric analysis, again, the filters were weighed thrice using the Sartorius Quintix 65-1S. Scanning Electron Microscope (SEM) was performed in secondary electron mode using a FEI Quanta 200F, to analyse particulates sampled on the MPS grids and from those images manual measurements were performed using ImageJ software. Energy-dispersive spectroscopy using a Xmas 150 by Oxford instruments was also performed in an attempt to analyse the chemical composition of the particulates.

2.3. Characterization of aerosolized particles

As discussed in Section 2.2, sampling of the effluents was performed by MPS and particles were captured on 3 mm circular copper Quantifoil 400 mesh/1.2 μm grids. Each Quantifoil grid consisted of over 400 × 37 μm^2 (Fig. 1(b)) sections, so selective grids were analysed to determine particle type, concentration, size and population. SEM was performed in secondary electron mode using a FEI Quanta 200F, energy-dispersive spectroscopy using a Xmas 150 by Oxford instruments and manual measurements of the particles (by measuring largest lengths) were performed using Image J software.

3. Results and discussion

3.1. Results from DLPI testing

Results for CFC, CFC_NC, CFC_LDH and CFC_NT during 75 kW/m^2 heat exposure only, and 16 J impact at TTI + 10 s during 75 kW/m^2 heat exposure are tabulated in Table 2. These results are the total mass loss due to the impact and heat exposure, the total mass captured from the sum of all DLPI filters and mass captured from sampling of the back face chamber (using methodology, discussed elsewhere (Chapple et al., 2021; Chapple, 2021)). As can be seen, the reproducibility of the results is very good. The mass of particles captured from the back surface for each sample though is very low despite considerable total mass loss. Since on exposure to 75 kW/m^2 samples self-ignited, a high percentage of the epoxy matrix and possibly some fibre sizing decomposed, becoming residual char, soot or volatiles, explaining 33–37% mass loss in all samples (Table 2). However, the composite sample lost stiffness, hence on impact a very little amount of particles was released on the back surface for each sample, as discussed in details elsewhere (Chapple et al., 2021; Chapple et al., 2022). The particles captured from the back-surface were not further analysed as these have also been already reported elsewhere (Chapple et al., 2021; Chapple et al., 2022). The TTI and FO values of all samples are given in Table 2. Images of all tested samples, back and front faces, are presented in Table 2, the particle-size mass distribution of soot and particles relevant to their aerodynamic diameter are provided in Fig. 3.

Once samples were exposed to heat, their damage mechanism during impact changed compared to sample subjected to impact only, as detailed in our previous studies (Chapple et al., 2021; Chapple et al., 2022). Some integral stiffness was lost during the thermal exposure of samples leading up to ignition, resulted in increased indentation damage and reduced fracturing, the opposite of that observed during impact only studies. The addition of nanomaterials promoted some charring, and the nanomaterials acted as reinforcements in the char, increasing char strength and hence, improving the impact resistance, most noticeable in CFC_NT samples.

3.2. Behaviour of samples during 75 kW/m^2 heat exposure and 16 J impact

Fire Behaviour of samples: The control CFC sample ignited at 54 ± 12 s and burned until 314 ± 13 s. The presence of NC and LDH reduced the TTI of CFC_NC and CFC_LDH compared to control CFC sample, as expected from standard cone calorimetry testing (Chapple, 2021). One of the CFC_LDH samples had a very high TTI during 75 kW/m^2 heat exposure, however, the damage was not very different. In addition, the presence of LDH slightly reduced burning duration (mainly during impact at TTI + 10 s during 75 kW/m^2 heat exposure). CFC_NT samples also had increased TTI and burning duration compared to CFC samples.

For all the samples, there was a significant increase in burning duration when samples were impacted and damaged. During many of the tests it was noticeable that a flame was present the longest, at the damage location and was the last area to flame out. This indicates that

Table 2
Quantitative analysis of the samples and particles captured during 75 kW/m^2 heat exposure and impact during 75 kW/m^2 heat.

Sample Composition	Heat flux (kW/m^2)	16 J Impact time (s)	TTI (s)	FO (s)	Burning duration (s)	Total mass loss		Captured in DLPI effluents*		Captured on BF filter*		Impact damage** (Test)
						(mg)	(%)	(mg)	(%)	(mg)	(%)	
CFC	75	–	54 ± 12	368 ± 1	314 ± 13	989 ± 22	33 ± 0	0.22 ± 0.063	0.007 ± 0.002	0.13 ± 0.13	0.004 ± 0.004	–
		TTI + 10	45 ± 8	441 ± 46	396 ± 38	989 ± 5	33 ± 0	0.163 ± 0.06	0.005 ± 0.002	3.25 ± 0.42	0.109 ± 0.013	B
CFC_NC	75	–	28 ± 4	436 ± 2	408 ± 2	978 ± 10	33 ± 0	0.129 ± 0.019	0.005 ± 0.001	1.36 ± 0.49	0.046 ± 0.016	–
		TTI + 10	34 ± 2	540 ± 80	506 ± 78	938 ± 23	33 ± 0	0.168 ± 0.025	0.006 ± 0.001	2.04 ± 2.04	0.071 ± 0.071	B (1) A (2)
CFC_LDH	75	–	139 ± 110	458 ± 22	319 ± 88	1026 ± 20	34 ± 0	0.164 ± 0.014	0.006 ± 0.001	0.79 ± 0.4	0.026 ± 0.013	–
		TTI + 10	40 ± 13	411 ± 19	371 ± 6	968 ± 17	32 ± 0	0.277 ± 0.09	0.009 ± 0.003	0.52 ± 0.34	0.018 ± 0.012	B (1) A (2)
CFC_NT	75	–	76 ± 3	469 ± 6	393 ± 9	1132 ± 17	37 ± 0	0.109 ± 0.029	0.004 ± 0.001	0.17 ± 0.17	0.006 ± 0.006	–
		TTI + 10	48 ± 15	505 ± 17	457 ± 2	986 ± 3	34 ± 0	0.10 ± 0.01	0.004 ± 0.001	1.52 ± 0.2	0.052 ± 0.007	A

TTI = time-to-ignition; FO = flame out.
* Percentage of total mass loss.
** Impact Damage Type: A = Splits/Cracks/Fibre Breakage B = Combined Large Cracks with Fibre Breakage, Indentation/Penetration.

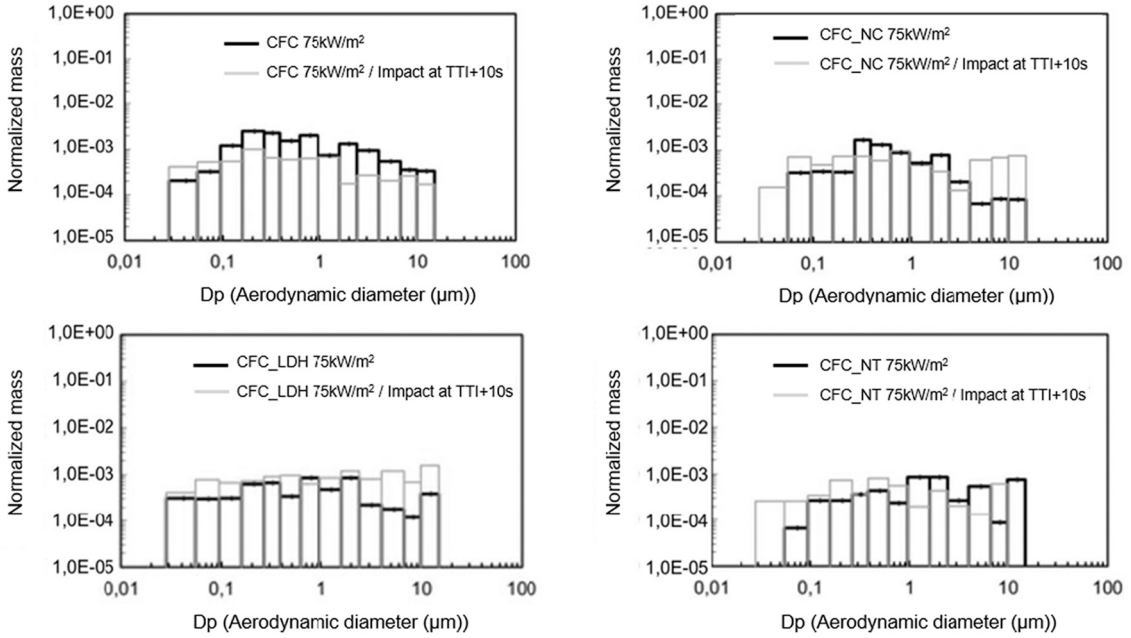

Fig. 3. Particle-size mass distribution of CFC, CFC_NC, CFC_LDH and CFC_NT samples in both 75 kW/m^2 heat exposure and impact at TTI + 10 s during 75 kW/m^2 heat exposure conditions.

the moderate damage allowed a slow release of the volatiles within the back face chamber. This event resembled the burning of a candle, with excess soot/particulate deposition clearly exemplified by one of the CFC samples presented in Fig. S2 a3. At the damage location some extracted fibres possibly coated with the polymer matrix, could have acted as a wick and the thermal conduction along the fibres promoted the release of polymer degradation products feeding the flame.

Damage analysis: The reduction in impact energy from 19 J reported elsewhere (Chapple et al., 2021; Chapple et al., 2022) to 16 J did stop extensive penetration damage of the samples, although both CFC, one CFC_NC and one CFC_LDHa had partial penetration. CFC_NTa samples provided the most impact resistance and no back face damage was visible. The addition of nanomaterials promoted charring, and the nanomaterials acted as reinforcements in the char, increasing char strength and hence, improving the impact resistance. This was again observed in these results.

Particle release: gravimetric analysis: There was no obvious significant difference in gravimetric results for the total amount of particulate mass captured on the DLPI filters from the different samples (Table 2). Throughout the testing, the amounts captured were very small, in the range of 0.003–0.012% of the total sample mass. In this study the soot in the effluents was diluted at the ratio 1:1000, resulting in only a very small percentage of the soot being sampled. Scaling the results by the dilution ratio (multiplying by 1000 resulting in a theoretical captured percentage of 3–12% of the total sample mass) presented an increased variation of particulate mass, captured from the effluents, between different samples. However, the highest percentage of total mass loss was 12% for CFC_LDH under impact during 75 kW/m^2 heat exposure and the second highest captured percentage of was 9% for CFC under 75 kW/m^2 heat exposure, indicating no significant trend from the introduction of nanomaterial additives.

The gravimetric results of the BF filter showed that the highest mass was captured from CFC control samples during fire and impact. These samples showed the least impact resistance and were most damaged, as presented in Table 2. CFC_NC and CFC_NT samples also had an increase in BF filter capture mass, during tests involving impact damage. Although their BF capture mass was reduced compared to the CFC control samples, correlating with their increased impact resistance and reduced damage. Moreover, CFC_LDH had a reduced BF captured mass during fire and impact tests, compared to fire only tests, even though one of the tests partially penetrated. However, for all the test results, only a small amount of mass was captured on the BF filters and although a trend of more extensive damage due to the impact event appears to result in increased mass on the back face filter, experimental error is a factor and likely the reason for the CFC_LDH result.

3.3. *Particle-size mass distribution emitted during fire exposure and impact*

The particle-size mass distribution was obtained by measuring the particle mass deposited on every impaction stage of the DLPI. Fig. 3 presents the logarithmic representations of mass distributions as a function of particle aerodynamic diameter (d_a) for each sample type during 75 kW/m^2 heat exposure and impact at TTI + 10 s during 75 kW/m^2 heat exposure. The Y axis, normalized mass ($dM/M_0 dlogd_a$), represents the relative mass M/M_0 of the collected particles divided by the measurement channels width in the logarithmic scale (Chivas-Joly et al., 2016).

In both 75 kW/m^2 heat exposure and impact at TTI + 10 s during 75 kW/m^2 heat exposure conditions, there was negligible difference in the mass distributions and the presence of nanomaterials additives presented no significance effect in the results. Comparing the distribution in the DLPI with the respiratory tract, particles were present that would deposit in all regions from the larynx to the alveoli (Fig. 4).

The percentiles (Table 3) of the cumulative particle-size mass distribution provides some more details of the percentage of particles that would be deposited in which regions of the respiratory tract. For all samples in both conditions except for CFC_LDH and CFC_NT during 75 kW/m^2 / Impact at TTI + 10 s, 50% of the particles sampled would deposit deep in the respiratory tract within the alveoli. Particles sampled up to 75% for all samples in both conditions would deposit in the lungs reaching the bronchi region at a minimum. The dispersion index ((D75-D25)/D50), characterises the width of the size distribution, low values of the index correspond to sharp distributions, whereas high values correspond to wide distributions. The distributions of particles are moderate in general, CFC_NC during only 75 kW/m^2 radiant heat exposure, had the sharpest distribution, however during 75 kW/m^2 / Impact at TTI + 10 s, CFC_NC had the widest distribution. As observed

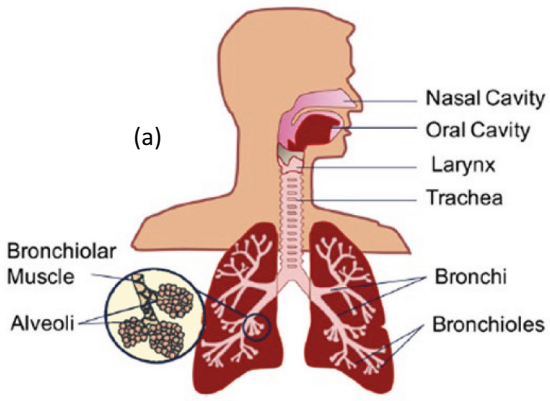

(b)

Region in the human respiratory tract	Respiratory tract size cut-off (μm)	DLPI stage
Nasal cavity	21.3	-
Oral cavity	14.8	-
Larynx	9.8	13
Trachea	6	12
Bronchi	3.5	11
Bronchioles	1.55	9
Alveoli	0.52	7

Fig. 4. (a) Respiratory tract and (b) relationship of DLPI stage with soot and particle size cut-off relative to the region of the respiratory tract they are deposited (Rhodes et al., 2011; Lodge Jr, 1987; Rubow et al., 1987). Reproduced with permission from (Rhodes et al., 2011).

Table 3
Percentiles of the cumulative particle-size mass distribution of CFC, CFC_NC, CFC_LDH and CFC_NT samples in both 75 kW/m^2 heat exposure and impact at TTI + 10 s during 75 kW/m^2 heat exposure conditions.

Sample and condition	D25 (μm)	D50 (μm)	D75 (μm)	Dispersion Index
CFC 75 kW/m^2	0.13	0.34	0.92	2.3
CFC 75 kW/m^2 / Impact at TTI + 10s	0.09	0.28	0.8	2.5
CFC_NC 75 kW/m^2	0.19	0.32	0.65	1.4
CFC_NC 75 kW/m^2 / Impact at TTI + 10s	0.12	0.43	2.69	6
CFC_LDH 75 kW/m^2	0.1	0.35	1.28	3.3
CFC_LDH 75 kW/m^2 / Impact at TTI + 10s	0.15	0.78	3.26	4
CFC_NT 75 kW/m^2	0.11	0.3	0.79	2.3
CFC_NT 75 kW/m^2 / Impact at TTI + 10s	0.34	0.91	2.64	2.5

with particle-size mass distributions (Fig. 3) the cumulative particle-size mass distribution (Fig. 5) also presents no significant effect in the results related to sample type or condition. From all samples, i.e., with or without nanomaterial additives, all released particles could be deposited deep in the respiratory tract.

3.4. Dimensional measurement of particles released using scanning electron microscopy (SEM)

Throughout all the SEM analyses of the particles captured on the grids of the MPS, predominantly soot particles were observed (Fig. 6). Spherical particles were also sometimes observed and a few larger lamellar particles which were concluded to be contamination. No pristine fibres and fibre fractions, resin particles or nanomaterial additives were observed throughout the analysis. It was concluded that fibres and resin particles were likely too large to be sampled by the MPS as its cut-off sampling size is 1 μm. Moreover, nanomaterial additives were likely contained within larger resin particles and not released separately. The soot particles observed were predominantly soot agglomerates formed by constituent (primary) soot (singular soot particles). Moreover, constituent soot particles were also identified separated in few instances.

Constituent (primary) soot particles: Although constituent soot particles were predominantly a component of soot agglomerates, there were still multiple examples of them as singular particles. Thus, their morphology was relevant for investigation. Measurements were taken from all clearly identifiable constituent soot particles both released singularly or as part of soot agglomerates for all sample types. There was no significant difference between the size and shape of the constituent soot particles sampled at ignition, mid-test and flame out (Fig. 6), thus all soot measurements were compiled together and tabulated into

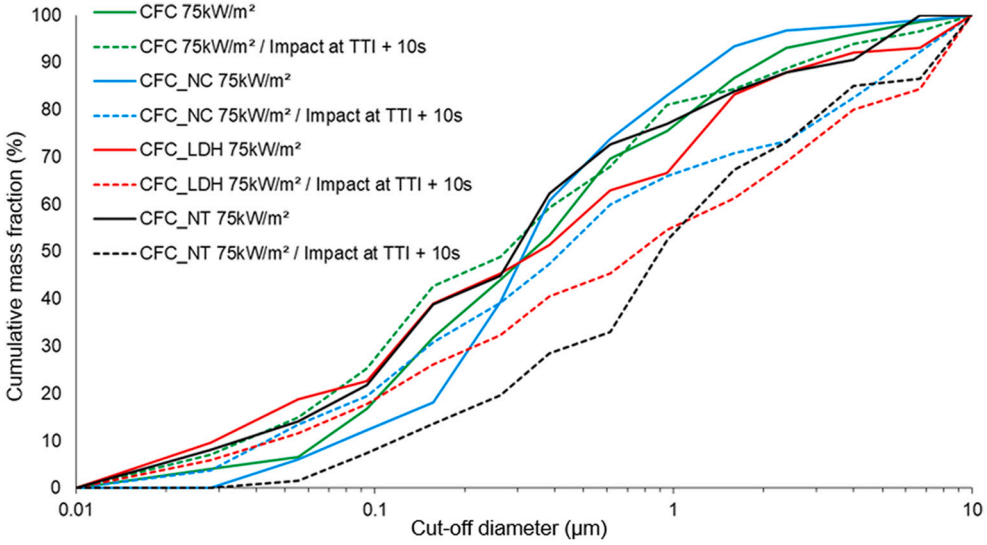

Fig. 5. Cumulative particle-size mass distribution of CFC, CFC_NC, CFC_LDH and CFC_NT samples in both 75 kW/m^2 heat exposure and impact at TTI + 10 s during 75 kW/m^2 heat exposure conditions.

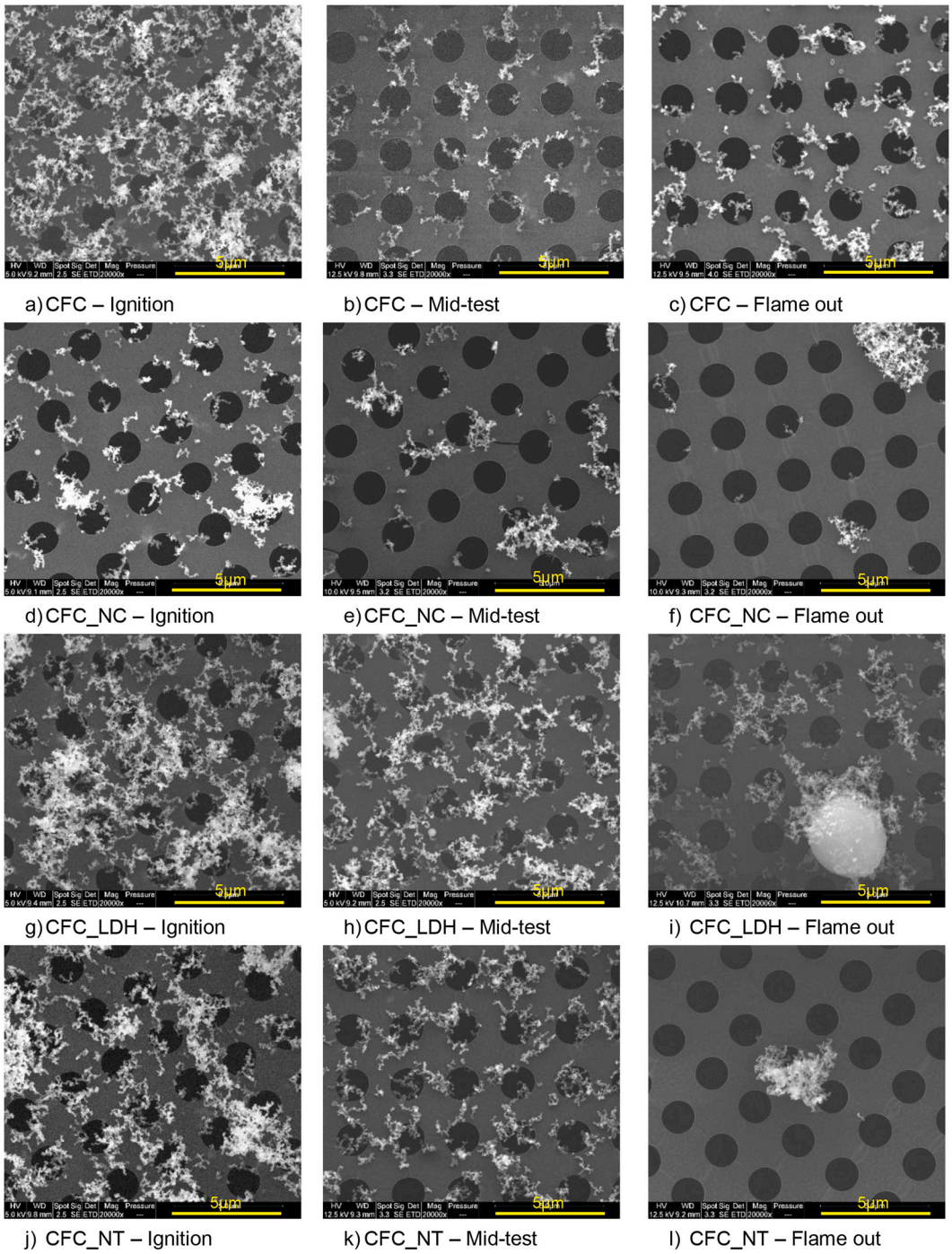

Fig. 6. Soot concentrations for each composition.

Table 4
Constituent soot particle size distribution of CFC, CFC_NC, CFC_LDH and CFC_NT samples in both 75 kW/m^2 heat exposure and impact at TTI + 10 s during 75 kW/m^2 heat exposure conditions.

Sample	Condition	Number of Soot Particles	Range (μm)	D25 (μm)	D75 (μm)	Dispersion Index	Median (μm)	Mode (μm)
CF	75 kW/m^2	425	0.04–0.18	0.08	0.11	0.36	0.09	0.09
	75 kW/m^2 / Impact at TTI + 10s	469	0.04–0.19	0.07	0.11	0.35	0.09	0.09
CF_NC	75 kW/m^2	225	0.03–0.14	0.07	0.1	0.3	0.08	0.09
	75 kW/m^2 / Impact at TTI + 10s	225	0.03–0.18	0.06	0.1	0.3	0.08	0.06
CF_LDH	75 kW/m^2	605	0.04–0.19	0.07	0.09	0.33	0.08	0.08
	75 kW/m^2 / Impact at TTI + 10s	279	0.03–0.15	0.07	0.1	0.35	0.08	0.09
CF_NT	75 kW/m^2	300	0.05–0.17	0.08	0.11	0.3	0.1	0.09
	75 kW/m^2 / Impact at TTI + 10s	185	0.04–0.13	0.06	0.09	0.42	0.07	0.07

sample type and condition (Table 4). Moreover, the shape of the constituent soot particles was spheroidal (irregular rounded shape) rather the perfectly spherical and their aspect ratio was approximately <2:1. All constituent soot particle measurements were below 0.2 μm and at their longest length, thus, the relevance of aspect ratio at such small dimensions was negligible. The statistical results of the constituent soot particle measurements are presented in Table 4.

All constituent soot particles measured were in the size range 0.03–0.15 μm with a variation in their median diameter of only 0.03 μm. The population (particles collected) data have been normalized with respect to size class, *K*, determined as $K = N^{1/2}$; where *N* is the number of nanoparticles in the study population.

The size distribution of constituent soot particles for all sample types were also similar (Fig. 7). Thus, as with the results of the DLPI, there was no significant difference between constituent soot particle size between samples with or without nanomaterial additives and between 75 kW/m^2 heat exposure only or impact at TTI + 10 s during 75 kW/m^2 heat exposure conditions.

The cut-off size of the MPS measurements was 1 μm, however, all constituent soot particle measurements were <0.19 μm. All constituent soot particles that were released individually were much less than the cut-off size of particles that can reach the alveoli region of the respiratory tract (Fig. 5). However, size is not the only parameter related to the deposition of particles in the respiratory tract, Brownian motion is also an important factor. Their chemical composition, surface chemistry and surface charge are the factors related to the resulting health effects. Moreover, such small particles (< 0.3 μm) could possibly remain airborne (Oberdörster et al., 2005).

Soot aggregates/agglomerates: To investigate the morphology of the soot aggregates/agglomerates, measurements of multiple soot aggregates/agglomerates along their longest length were performed manually using ImageJ from CFC control samples exposed to 75 kW/m^2 radiant heat only during ignition, mid-test and flame out. The statistical results and population of these soot agglomerate measurements are presented in Fig. 8. The aggregates/agglomerates observed were formed as many random shapes and in some instances of dense concentration or exceeding the grid section boundaries, as shown in Fig. 6, making them difficult to measure. The aggregates/agglomerates that could be measured were in a size range that could deposit in the respiratory tract, in which 75% of the aggregates/agglomerates could deposit deep in the lung in the bronchioles and >25% in the alveoli (Fig. 5). Some aggregates/agglomerates in a size range less likely to remain airborne could potentially be more likely to deposit deep in the lung than some constituent soot particles that possibly could remain airborne and be exhaled. All the soot aggregates/agglomerates were smaller than the diameter of the macrophage cells in the alveoli, thus they will be effectively removed via phagocytosis unless the composition of the soot

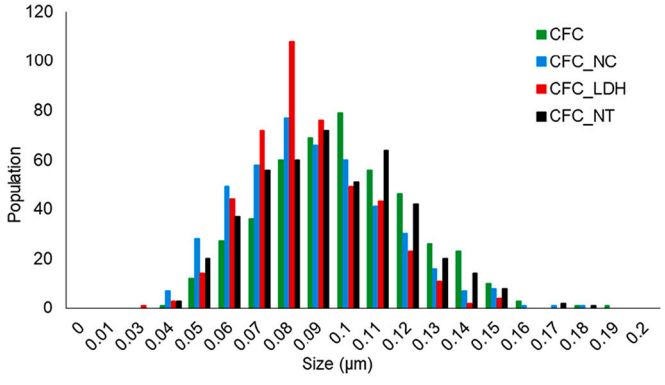

Fig. 7. Population of all combined constituent soot particle measurements from both 75 kW/m^2 heat exposure and impact at TTI + 10 s during 75 kW/m^2 heat exposure conditions for CFC, CFC_NC, CFC_LDH and CFC_NT samples.

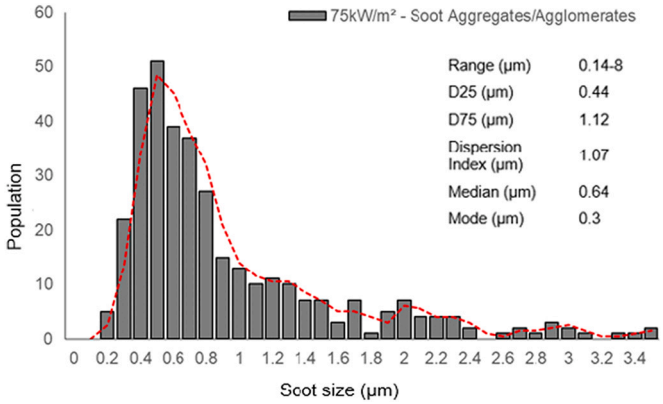

Fig. 8. Population of soot aggregates/agglomerates from 75 kW/m^2 heat exposure for CFC.

adversely affects the macrophages.

Soot concentration: The concentration of soot did reduce at mid-test and flame out sampling, most noticeably for CF_NC and CFC_NT samples. This reduction correlates to the SPR data presented in Fig. 2. SEM images presented in Fig. 6 also show a reduction in soot concentration during mid-test sampling and a further reduction in concentration at flame out. This reduction in concentration had no significant impact on the size or shape of constituent soot particles, however, there could be some significance related to soot agglomerate size and respirability. A dense concentration of soot potentially enables the formation of larger aggregates/agglomerates, and so have reduced respirability. Therefore, a reduced concentration could possibly result in an increased number of respirable aggregates/agglomerates. However, alternatively there could still be a greater number of respirable aggregates/agglomerates in addition to non-respirable aggregates/agglomerates in a dense concentration compared to a reduced concentration.

Composition of soot: To investigate the chemical composition of soot, energy-dispersive spectroscopy was performed on a dense soot agglomerate released from a CFC sample. The soot agglomerate was porous and only the composition of the Quantifoil grid was identified (Fig. S3 (a)). There was also little difference in the spectral peaks (Fig. S3 (b)), thus the composition of the soot could not be established. To further investigate the chemical composition of soot, established methods such as neutron activation analysis or X-ray fluorescence analysis could be implemented (Adams, 2002), which will be focus of the future work.

4. Conclusions

To investigate the sub-micron sized particles released in effluent during impact and fire conditions, a DLPI and MPS set-up was combined with the bespoke impact and fire equipment. This set-up provided a mechanism for the capture of and determination of the aerodynamic size distribution of the released particles directly by mass and these results were then used to predict the regions in the respiratory tract in which the particles would deposit. The methodology for impact and fire test conditions were similar to that previously described (Chapple et al., 2021; Chapple et al., 2022) with the additional operations required for the DLPI and MPS system.

There was negligible difference between particle-size mass distribution of particles captured on DLPI filters for both 75 kW/m^2 heat exposure only and impact at TTI + 10s during 75 kW/m^2 heat exposure conditions and no significant effect from the addition of nanomaterial in the samples. Released particles were mainly from the matrix and no pristine NPs have been observed after fire and impact in soot. However, the results showed that the particles released could be deposited in all regions of the respiratory tract from the larynx to the alveoli, deep in the

lung. The percentiles of the cumulative particle-size mass distribution of the DLPI filters, showed that up to 75% of the soot and particles released could deposit in the lungs reaching the bronchi region at a minimum.

Investigating the morphology of the released particles by SEM showed only soot particles were captured on the MPS grids. No fibres/fibre fractions, resin particles or nanomaterial additives were observed, most likely because they were in excess of the 1 μm MPS cut-off sampling size. There was no difference in the size and shape of constituent soot particles regarding sample type or test condition. All constituent soot particle measurements were <0.19 μm, much less than the cut-off size of particles that can reach the alveoli region of the lung. In addition, 75% of soot aggregates/agglomerates released from CFC sample during 75 kW/m^2 heat exposure could deposit deep in the lung in the bronchioles and alveoli.

CRediT authorship contribution statement

R. Chapple: Conceptualization, Methodology, Investigation, Formal analysis, Writing – original draft. **C. Chivas-Joly:** Data curation, Writing – review & editing. **J.-C. Roux:** Investigation. **L. Dumazert:** Investigation. **L. Ferry:** Supervision, Writing – review & editing. **J.-M. Lopez-Cuesta:** Conceptualization, Resources, Supervision, Writing – review & editing, Funding acquisition. **E.L. Erskine:** Writing – review & editing. **B.K. Kandola:** Conceptualization, Visualization, Writing – original draft, Funding acquisition, Supervision, Project administration.

Declaration of Competing Interest

The authors declare that they have no known competing financial interests or personal relationships that could have appeared to influence the work reported in this paper.

Data availability

Data will be made available on request.

Acknowledgements

The authors acknowledge the Dstl, UK for the financial and technical assistance (Contract No: DSTLX-1000106109); Bitrez Ltd. UK for supply of the resin and Ocsial, EU for NT. Technical support from J. Milnes from Bolton during equipment designing; Aziliz Calvez from Bolton for sample preparation; J-C Roux from IMT Ales for SEM study; and F. De Lagos from LNE during equipment setup, is much appreciated.

Appendix A. Supplementary data

Supplementary data to this article can be found online at https://doi.org/10.1016/j.impact.2022.100446.

References

Adams, F., 2002. Chemical characterization of atmospheric particles. In: International Atomic Energy Agency Conference, Seibersdorf, Austria, pp. 36–54.
Bai, J., 2003. Carbon 41 (6), 1325–1328.
Chapple, R., Kandola, B.K., Myler, P., Ferry, L., Lopez-Cuesta, J.-M., Chivas-Joly, C., Erskine, E.L., 2021. Polym. Compos. 42, 6127–6145.
Chapple, R., 2021. PhD thesis University of Bolton.
Chapple, R., Ferry, L., Lopez-Cuesta, J.-M., Chivas-Joly, C., Erskine, E.L., Kandola, B.K., 2022. Environ. Sci. Nano 9, 3957–3972.
Chivas-Joly, C., Saragoza, L., Motzkus, C., 2013. Mod. Polym. Mater. Environ. Appl. 5, 67–78.
Chivas-Joly, C., Gaie-Levrel, F., Motzkus, C., Ducourtieux, S., Delvallée, A., De Lagos, F., Lopez-Cuesta, J.-M., 2016. J. Hazard. Mater. 301, 153–162.
Chivas-Joly, C., Longuet, C., Pourchez, J., Leclerc, L., Sarry, G., Lopez-Cuesta, J.-M., 2019. J. Hazard. Mater. 365, 405–412.
Costantino, J., Jarbeau, J.J., Hintz, T.J., Hinojosa, M., Edwards, C.W., Batten, T.W., Black, J.E., 2015. Composite material hazard assessment at crash sites. In: Wright-Patterson Air Force Base, Ohio 45433–7913: Air Force Research Laboratory, 2001. Report updated AFRL-SA-WP-SR-2015–0011.
Dekati, 2022. DLPI Low Pressure Impactor brochure. Available at. https://www.ecotech.com/wp-content/uploads/2015/03/Dekati-DLPI.pdf (Accessed 13/06/2022).
Fleury, D., R'Mili, B., Janes, A., Vignes, A., Bomfim, J.A.S., Sinesi, S., Bouillard, J.X., 2011. New Evidence Towards the Release of Airborne Carbon Nanotubes when Burning Nanocomposite Polymers, vol. 1. National Institute of Standards and Technology, Nanotech, Boston US. ISBN 978-1-4398-7142-3,.
Gandhi, S., 1999. Aviat. Fire. J. 6.
Gandhi, S., Lyon, R., Speitel, L., 1999. J. Fire Sci. 17, 20–41.
Hertzberg, T., 2005. Fire Mater. 29, 231–248.
Holmes, M., 2014. Reinf. Plast. 58 (6), 38–45.
International Organization for Standardization, ISO 29904:2013, 2013. Fire Chemistry - Generation and Measurement of Aerosols.
International Organization for Standardization, ISO/TS 27,687:2008, 2008. 2008 Nanotechnologies. Terminology and Definitions for Nano-Objects. Nanomaterials, Nanofibre and Nanoplates.
Kalali, E.N., Wang, X., Wang, D.Y., 2016. J. Mater. Chem. A 4 (6), 2147–2157.
Kandola, B.K., Deli, D., 2014. In: Papaspyrides, C.D., Kiliaris, P. (Eds.), Polymer Green Flame Retardants. Elsevier Science and Technology, Amsterdam, p. ch 16.
Kandola, B., Kandare, E., 2008. In: Horrocks, A.R., Price, D. (Eds.), Advances in Fire Retardant Materials. Woodhead Publishing, Cambridge, pp. 398–442.
Kulkarni, P., Baron, P.A., Willeke, K., 1993. Aerosol Measurement. Principles, Techniques and Applications. J. Wiley & Sons, New Jersey US. ISBN 0–471–28406-8. ISBN: 978–0–470-38741-2.
La Delfa, G., Luinge, J.W., Gibson, A.G., 2009. Plast. Rubber Compos. 38, 111–117.
Li, Z., Wang, Y., Cao, J., Meng, X., Aamir, R.M., Lu, W., Suo, T., 2020. Compos. B. Eng. 200, 108270.
Liu, Q., Zhou, X., Fan, X., Zhu, C., Yao, X., Liu, Z., 2012. Polym.-Plast. Technol. Eng. 51 (3), 251–256.
Lodge Jr., J.P., 1987. Atmos. Environ. 21 (10), 2265–2266.
Majoral, C., Pape, A.L., Diot, P., Vecellio, L., 2006. Aerosol Sci. Technol. 40, 672–682.
Martins, M., Schartel, B., Magalhães, F., Pereira, C., 2016. Fire Mater. 41, 111–130.
Morrey, E.L., 2001. PhD Thesis, Centre for Composite Materials. Imperial College of Science, Technology and Medicine, London UK.
Motzkus, C., Chivas-Joly, C., Guillaume, E., Ducourtieux, S., Saragoza, L., Lesenchal, D., Mace, T., 2010. Characterization of aerosols emitted by the combustion of nanocomposites. In: Conference NanoSafe, Grenoble France.
Mouritz, A.P., Gibson, A.G., 2006. Fire Properties of Polymer Composite Materials. Springer, Dordrecht, pp. 359–382.
Ning, N., Wang, M., Zhou, G., Qiu, Y., Wei, Y., 2022. Compos. B. Eng. 234, 109749.
Nyden, M.R., Harris, R.H., Kim, Y.S., Davids, R.D., Marsh, N.D., Zammarano, M., 2009. Characterizing Particle Emission from Burning Composites. National Institute of Standards and Technology, Nanotech, Huston US.
Oberdörster, G., Maynard, A., Donaldson, K., Castranova, V., Fitzpatrick, J., Ausman, K., Carter, J., Karn, B., Kreyling, W., Lai, D., Olin, S., Monteiro-Riviere, N., Warheit, D., Yang, H., 2005. Part. Fibre. Toxicol. 2, 8–35.
Owen, P.E., Glazier, J.R., Ballantyne, B., Clary, J.J., 1986. J. Occup. Med. 28 (5), 373–376.
Rhodes, J., Smith, C., Stec, A.A., 2011. Polym. Degrad. Stab. 96 (3), 277–284.
Rubow, K.L., Marple, V.A., Olin, J.G., McCawley, M.A., 1987. Am. Ind. Hyg. Assoc. J. 48 (6), 532–538.
Schlagenhauf, L., Kuo, Y.Y., Bahk, Y.K., Nuesch, F., Wang, J., 2015. J. Nanopart. Res. 17, 440.
Shettar, M., Kowshik, C.S.S., Manjunath, M., Hiremath, P., 2020. J. Mater. Res. Technol. 9 (4), 9108–9116.
Shrivastava, R., Singh, K.K., 2020. Polym. Rev. 60, 542–593.
Singh, D., Sotiriou, G.A., Zhang, F., Mead, J., Bello, D., Wohlleben, W., Demokritou, P., 2016. Environ. Sci. Nano 3 (6), 1293–1305.
Sotiriou, G.A., Singh, D., Zhang, F., Wohlleben, W., Chalbot, M.G., Kavouras, I.G., Demokritou, P., 2015. Environ. Sci. Nano 2 (3), 262–272.
Souto, F., Calado, V., Pereira Jr., N., 2018. Mat. Res. Expr. 5, 072001.
Thomson, S.A., Hilaski, R.J., Wright, R., Mattie, D., 1990. Nonrespirability of carbon fibers in rats from repeated inhalation exposure. In: Wright-Patterson Air Force Base, Ohio 45433: Chemical Research Development and Engineering Center, Aberdeen Proving Ground, MD. Report AD-A228–196/HDT.
Warheit, D.B., Hansen, J.F., Carakostas, M.C., Hartsky, M.A., 1994. Am. Occup. Hyg. 38, 769–776.
Waritz, R.S., Collins, C.J., Ballantyne, B., Clary, J.J., 1990. Toxicologist. 19, 70–71.
Winter-Sorkina, R.D., Cassee, F.R., 2002. From concentration to dose: factors influencing airborne particulate matter deposition in humans and rats. Dutch Nat. Inst. Publ. Health Environ. Rep. 1–36.
Zabihi, O., Ahmadi, M., Nikafshar, S., Chandrakumar Preyeswary, K., Naebe, M., 2018. Compos. B. Eng. 135, 1–24.
Zhang, Z., Wang, X., Lin, L., Xing, S., Wu, Y., Li, Y., Wu, L., Gang, B., 2006. J. Occup. Health 43 (2), 75–79.
Zhang, R.L., Gao, B., Du, W.T., Zhang, J., Cui, H.Z., Liu, L., Ma, Q.H., Wang, C.G., Li, F. H., 2016. Comp. Part A 84, 455.